Measurements in Vertical Plane Turbulent Plumes

B. R. Ramaprian
Professor of Mechanical and Materials Engineering, Washington State University, Pullman WA.
Mem. ASME

M. S. Chandrasekhara
Adjunct Research Professor, Department of Aeronautics and Astronautics, Naval Postgraduate School, Monterey, CA
Assoc. Mem. ASME

Mean-flow and turbulence measurements have been obtained in two-dimensional vertical turbulent plumes in a nominally still ambient. The plumes were generated by injecting hot water vertically upwards from the bottom of a reservior containing cold water. A two-component Laser Doppler Anemometer (LDA) and a "cold-film" resistance thermometer were used to obtain instantaneous velocity and temperature measurements in the plume. The present mean-flow measurements have confirmed many of the earlier measurements on plane plumes, but have also indicated some important differences. The use of the two-component LDA made it possible to obtain data on turbulent intensities, turbulent fluxes and other details of the structure of turbulence in plane plumes. The turbulence measurements have shown that the eddy viscosity and turbulence are significantly higher in the plume compared to an isothermal jet. Detailed measurements of energy balance suggest that buoyant production contributes substantially to this increase.

Introduction

There are several practical applications for the study of turbulent plumes, for example, cooling-tower and chimney exhausts, and hot-water discharges from power plants to lakes and rivers. The plume is also an interesting complex flow in which turbulent motions are strongly influenced by buoyancy. Study of the plume may lead to a better understanding of the role of buoyancy in turbulent shear flows. Early methods of prediction of buoyant jets were based on the well-known integral techniques [1–4] using empirical physical assumptions about the flow (e.g., the value of an entrainment coefficient). More recent methods [5–8] involve solution of the complete set of governing partial differential equations using turbulence models of varying degrees of complexity.

The empirical input required in either of the above approaches is to be obtained from detailed experiments. There have been only a few such experiments reported in the literature. These include the early experiments such as those of Rouse, Yih, and Humphreys [9] on round and plane plumes, and Lee and Emmons [10] on a plane plume; the more recent round-plume experiments [11–13] and the plane buoyant-jet and plume experiments of Kotsovinos [14] reported in [15]. Of the above, the experiments of Kotsovinos represent the only extensive study on plane buoyant jets and plumes, reported in the literature. These experiments were performed in water using a one-component Laser Doppler Anemometer (LDA) for instantaneous velocity measurements and a microthermistor for temperature measurements. Extensive as the work was, the single-component LDA used in [14] did not allow the direct measurement of the turbulent transport of momentum and heat in the cross-stream direction. While detailed data of these turbulent fluxes are available for the round plume from [13], similar information is not available for the plane plume. The present experiments were designed primarily to obtain this information for the plane plume. In the present experiments, as in those of Kotsovinos and List [15] (referred to henceforth as KL) heat was used to produce buoyancy. A two-component LDA system, coupled with a microresistance thermometer (cold film) was used to measure two instantaneous velocity components U and V and the instantaneous temperature excess ΔT above the ambient. The study was focused on the asymptotic plume rather than on the entire range of buoyant-jet flows. This was done because the asymptotic plume is independent of the initial conditions and hence, represents a well-defined flow configuration. It is, therefore, ideal both for the study of buoyancy effects on turbulence and for use as a basic test case in the development of predictive models for buoyancy-driven flows.

Experimental Conditions and Procedure

The experiments were conducted in a hydraulic flume 7 m long × 0.45 m wide × 0.75 m deep, which served in the present experiments, simply as a large reservior. A nozzle 5 mm in width (D) and 250 mm in span, located at the bottom of the flume served as the source of the two-dimensional vertical submerged buoyant jet. The flow was confined between two plexiglas false side walls spaced 250 mm apart, to improve the two-dimensionality of the flow. The two-component LDA used had a spatial resolution of about 1.1 mm in the spanwise direction and 0.1 mm in the other two directions. The temperature sensor was located within about 1 mm downstream of the center of the focal volume of the LDA. The experimental apparatus, instrumentation and procedure were identical to those used for the study of nonbuoyant jets reported in [16]. Special problems associated with LDA measurements in a nonisothermal flow and with the contamination of the ambient by the heated fluid, as well as the

Contributed by the Fluids Engineering Division for publication in the JOURNAL OF FLUIDS ENGINEERING. Manuscript received by the Fluids Engineering Division June 17, 1987.

means to assess and minimize these problems are also described in that paper. These will not, therefore, be discussed here. Note that the measurements extended up to a height of 60 D above the nozzle exit and that the last measurement station was about 60 D below the free surface. The results for the plane jet presented in [16] also showed that there are no significant free-surface effects on the flow in the region of measurements.

Flow rate through the nozzle was measured using an orifice meter. The temperature of the jet fluid T_j and the ambient T_a were measured using thermistors. The flow rate was maintained constant to within 1 percent and the temperature excess $\Delta T_j (= T_j - T_a)$ to within 5 percent over the duration of the experiment. Their average values were used to define the (span averaged) *nominal* exit conditions for velocity, temperature excess and fluxes of mass, momentum, buoyancy and heat. It may be noted that the accurate knowledge of the exit conditions is not essential for the study of the asymptotic plume and that the exit conditions have been used only for either nondimensionalizing the data or deriving a length scale *representative* of the axial distance at which the flow can be expected to transform to the asymptotic plume state. The nominal values of these exit conditions are adequate for this purpose. The experiments pertained to four cases of plume flows. These are designated as MSC3, MSC3X, MSC3Y and MSC4. The nominal exit conditions corresponding to the flows are as shown in Table 1. The coefficient of thermal expansion of water, α in the above table, was obtained from the following expression suggested in [14]:

$$\alpha = (-0.073 + 0.19T - 0.0027T^2 + 0.00002T^3) \times 10.^{-4} \quad (1)$$

where T is the temperature of the water in degrees centigrade. R_j is the exit Richardson number defined by

$$R_j = \frac{\alpha g \Delta T_j D}{U_j^2} \quad (2)$$

Table 1 Experimental conditions

Flow Designation	U_j cm/s	ΔT_j °C	T_a °C	$\alpha_j \times 10^4$ $(^\circ C)^{-1}$	R_j
MSC3	10	23.2	24.4	4.42	0.050
MSC3X	10	19.0	21.0	3.85	0.036
MSC3Y	10	22.0	22.4	4.18	0.045
MSC4	5	22.3	21.1	4.10	0.179

Even though the flows MSC3X and MSC3Y do not differ significantly in their exit conditions from MSC3, these experiments were performed on different days and can therefore be used to ascertain the repeatability of the experimental results. The exit conditions in all the cases were such as to cause the laminar flow to become unstable almost immediately after exit (say within $x/D = 1$), as observed from dye visualization tests. Transition to turbulence can be expected to have been complete typically in the range $20 < x/D < 30$, as inferred from the transition criterion of Bill and Gebhart (see List [17]), namley the Grashoff number Gr at the transition point x_{tr} is given by

$$\mathrm{Gr} = g x_{tr}^3 \alpha (\Delta T_m)/\nu^2 = 3 \times 10^8 \quad (3)$$

Thus the plumes studied can be expected to be turbulent over most of the measurement range. It will also be shown that all the flows reached practically the asymptotic *turbulent* plume state by $x/D = 30$ with regard to the mean, and by $x/D = 40$ with regard to *most* turbulent properties. They, however, exhibited mild evolving trends in respect of some *details* of the turbulent structure in the measurement range $30 < x/D < 60$. The conservation of the (kinematic) heat flux integral H, defined by the two-dimensional, integral energy equation

$$H = \int_{-\infty}^{+\infty} (U \Delta T)\, dy = \int_{-\infty}^{+\infty} (\bar{U} \Delta \bar{T} + ut)\, dy \quad (4)$$

is a good test of not only the two-dimensionality of the flow in the neighborhood of the measurement plane, but also the

Nomenclature

B = kinematic buoyant force, $\int_{-\infty}^{+\infty} -\frac{\Delta\gamma}{\rho}\, dy$

b = half width, defined as the value of y at $\bar{U} = \frac{U_m}{2}$ $\left(\text{or at } \Delta\bar{T} = \frac{\Delta T_m}{2}\right)$

C_E = entrainment coefficient (equation (23))

C_p = growth parameter (equation (20))

D = jet width at exit

Gr = Grashoff number (equation (3))

g = acceleration due to gravity

H = kinematic heat flux (mean + turbulent)

K_1 = spreading rate $\frac{db}{dx}$ (equation (11))

M = kinematic momentum flux (equation (7))

M^* = nondimensional momentum flux (equation (8))

Pr = Prandtl number

Q = kinematic mass flux (equation (6))

Q^* = nondimensional mass flux (equation (19))

q = square root of turbulent kinetic energy per unit mass

R = Richardson number (equation (5))

T = temperature

ΔT = excess temperature above the ambient

ΔT_m^* = nondimensional maximum excess temperature (equation (24))

t = temperature fluctuation

U = axial velocity component

u = turbulent fluctuation in U

V = cross-stream velocity component

v = turbulent fluctuation in V

w = turbulent fluctuation in the spanwise direction

x = axial coordinate

x^* = nondimensional axial coordinate, $x\beta_j^{2/3}/M_j$

y = cross-stream coordinate

α = coefficient of thermal expansion

β = kinematic buoyancy flux (equation (8))

ϵ = rate of dissipation of turbulent kinetic energy (equation (28))

γ = specific weight

$\Delta\gamma$ = excess specific weight above the ambient

η = y/b

ρ = density

σ = coefficient

ν = kinematic viscosity

Subscripts

a = ambient

max, m = maximum value

cl = centerline of the jet

j = jet exit

M = pertaining to momentum

o = virtual origin

t = pertaining to temperature

u = pertaining to velocity

30 = pertaining to station $x/D = 30$

Other Notations

overbar = time-mean value

prime = rms value

Table 2 Experimental data of mean-flow properties

Flow designation and virtual origins (x_{oM}/D; x_{ot}/D)	$\frac{x}{D}$	ΔT_j	M	Q	β	B	H	b_u	b_t	U_m	ΔT_m	R
		°C	cm^3/s^2	cm^2/s	cm^3/s^3	cm^2/s^2	$\frac{cm^2 - °C}{s}$	cm	cm	cm/s	°C	
Uncertainties:	±0.005	±0.20	±4.0	±0.50	±1.00	±0.70	±2.0	±0.05	±0.05	±0.25	±0.20	±0.040
MSC3X	30	21.80	122.8	24.50	31.90	7.03	114.5	2.04	2.84	7.01	5.47	0.253
(−1.0; −6.0)	40	21.60	159.7	31.45	31.71	7.25	117.1	2.24	3.00	6.68	4.18	0.242
	50	22.20	168.1	37.30	28.35	6.70	107.0	2.54	3.52	6.41	3.37	0.310
	60	21.80	225.7	49.80	31.71	6.57	125.3	3.44	4.69	6.58	3.00	0.340
MSC3Y	30	19.55	115.9	24.96	29.70	7.04	111.3	1.80	2.24	6.60	5.41	0.297
(0.0; −5.0)	40	18.63	131.1	30.47	25.85	6.36	102.1	2.32	3.16	6.09	4.06	0.325
	50	19.96	185.3	38.93	33.43	7.27	132.1	2.77	3.26	6.53	4.01	0.310
	56	19.09	179.3	40.60	30.59	7.59	122.8	3.14	4.52	6.19	3.49	0.355
MSC3	20	23.40	119.7	19.90	47.20	8.69	145.8	1.24	1.51	8.13	8.67	0.216
(−4.0; −5.0)	30	22.80	160.6	28.00	43.78	8.32	139.5	1.72	1.96	7.97	6.15	0.232
	40	23.20	185.5	33.20	39.34	7.09	133.7	2.16	2.46	7.58	4.79	0.225
	50	23.30	240.0	44.90	41.79	8.27	144.4	3.25	3.77	7.26	3.76	0.273
	60	23.40	296.0	53.50	39.80	6.96	137.5	3.52	3.80	7.78	3.23	0.235
MSC4	30	22.39	76.8	17.20	25.60	6.66	89.99	1.50	1.87	5.69	6.19	0.287
(6.0; 6.0)	40	22.29	90.0	22.20	20.30	5.60	76.60	1.93	2.28	5.51	4.52	0.305
	50	22.46	113.0	28.40	17.65	5.73	70.50	2.23	2.60	5.60	3.54	0.280
	56	21.85	87.0	27.70	9.22	2.67	40.90	2.35	2.33	4.96	2.39	0.298

absence of any stratification of the ambient. Figure 1 shows results for the different flows in the measurement range $20 < x/D < 60$. The data are normalized using the value of H at $x/D = 30$. It is seen that flows MSC3 and MSC3X are reasonably two-dimensional and are free from any significant stratification effects. The result for flow MSC3Y is marginally acceptable. The flow MSC4 was particularly difficult to set up and measure, because of very low velocities and very large temperature fluctuations associated with this flow. It is possible that three-dimensional and stratification effects were present in this flow. Even so, some results from this experiment are presented to demonstrate that flows originating from substantially different initial conditions evolve towards the same asymptotic plume state. The experimental uncertainties in the case of the other three flows are: $\bar{U} = \pm 2.5$ mm/s; $\Delta\bar{T} = 0.2°C$; u', v', $t' = 5$ percent; $\overline{uv}$, $\overline{ut}$, $\overline{vt} = 10$ percent; $\overline{u^2 v}$, $\overline{v^3} = 15$ percent. Uncertainty estimates for the other derived quantities were obtained from an error-propopagation analysis in some cases and from the standard deviation of the data, in the other cases. These are indicated on the respective figures.

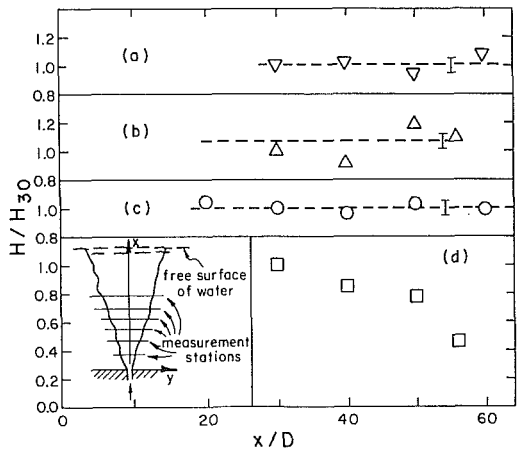

Fig. 1 Conservation of kinematic heat flux. (a) MSC3X, (b) MSC3Y, (c) MSC3, (d) MSC4. Dashed lines represent mean through data. Vertical bars represent uncertainty in the measurements.

Theoretical Framework

The theoretical framework for the analysis of the asymptotic plume has been well developed in the earlier literature [9, 15] and also briefly reviewed by List [17]. A dimensionless number often used to characterize plane vertical buoyant jets is the Richardson number R, which following KL, is defined as

$$\mathrm{R}(x) = (Q/M)^3 \beta \tag{5}$$

with

$$Q = \int_{-\infty}^{+\infty} \bar{U} dy \tag{6}$$

$$M = \int_{-\infty}^{+\infty} \overline{U^2} = \int_{-\infty}^{+\infty} (\bar{U}^2 + \overline{u^2}) dy \tag{7}$$

$$\beta = -\int_{-\infty}^{+\infty} \frac{1}{\rho} \overline{U \Delta\gamma} dy = -\int_{-\infty}^{+\infty} \frac{1}{\rho} (\bar{U}\Delta\bar{\gamma} + \overline{u\Delta\gamma'}) dy \tag{8}$$

being the kinematic fluxes of mass, momentum and buoyancy, respectively. All heated jets can be expected to reach eventually an asymptotic state in which all the flow properties assume selfsimilar distributions. Under such conditions, it can be shown [9] that the behavior of a fully turbulent plume is completely described by specifying only the initial kinematic buoyancy flux β_j defined by

$$\beta_j = \alpha_j g H_j \tag{9}$$

and that the following functional relationships can be written for such a plume:

$$\mathrm{R} = \text{constant} \tag{10}$$

$$b = K_1 x \tag{11}$$

$$Q = \sigma_Q \beta_j^{1/3} x \tag{12}$$

$$M = \sigma_M \beta_j^{2/3} x \tag{13}$$

$$U_m = \sigma_u \beta_j^{1/3} \tag{14}$$

and

$$\alpha g \Delta T_m = -\frac{\Delta\gamma_m}{\rho} = \beta_j^{2/3} / (x \sigma_t) \tag{15}$$

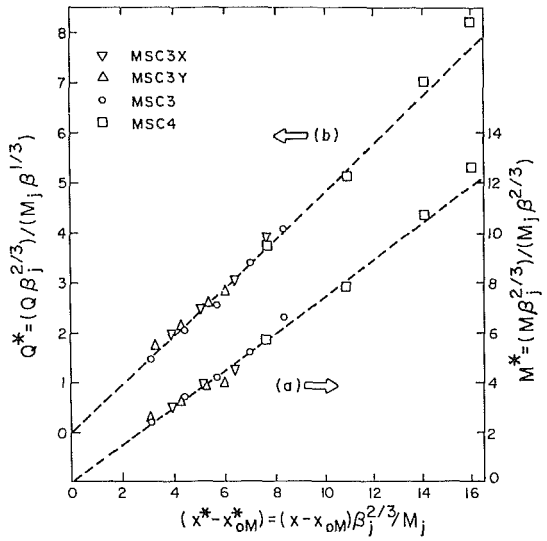

Fig. 2 Variations of kinematic fluxes of mass and momentum. Symbols as in Figs. 1. Uncertainties: x^*: ±0.3; Q^*: ±2.2 percent; M^*: ±3.3 percent.

where b is a characteristic width of the plume (usually the half-width), and K_1, σ_Q, σ_M, σ_u and σ_t are universal constants.

The above relations are based on the assumption of conservation of buoyancy flux in the plume, which is equivalent to the assumption of constant α, since heat flux is unconditionally conserved. In practice, there may be a significant decrease in the buoyancy flux with downstream distance in the near-field of the source, because of the rapid decrease in temperature (and hence α) along the plume axis. But changes in buoyancy flux will be very small in the far field (see for example Table 2). In such cases, it is still reasonable to assume that the above relationships will be valid, provided one uses, instead of the initial buoyancy flux β_j, the local buoyancy flux $\beta(x)$ defined in equation (8), which can also be written as

$$\beta = \int_{-\infty}^{+\infty} \alpha(x) g(\Delta\bar{T}\bar{U} + \overline{ut}) dy \tag{16}$$

It was found adequate in the present studies to assume a constant average value $\alpha(x)$ (equal to the value at the plume centerline) across the asymptotic plume ($x/D \geq 30$) without introducing substantial error into the evaluation of β.

Results and Discussion

Mean Flow Properties. Table 2 gives a summary of the important measured mean-flow properties. Note that the quantities M and β will be referred to as "mean-flow" quantities, even though they contain turbulent contribution. It is seen from Table 2 that except in the downstream part of MSC4 the buoyancy flux β remains reasonably constant (to within 10 percent) in the range $30 < x/D < 60$.

Kinematic Fluxes of Momentum and Mass. The experimental data on the kinematic momentum flux $M(x)$ obtained for each of the different flows were found to exhibit, within experimental scatter, a linear variation with axial distance of the form

$$M = A(x - x_{oM}) \tag{17}$$

where A is a constant and x_{oM} is the location of the virtual origin for each flow. Figure 2(a) shows a plot of the momentum-flux data for all the flows in normalized coordinates. The axial coordinate x^* chosen is suggested by KL. Hence, $(x^* - x^*_{oM})$ is the ratio of the distance $(x - x_{oM})$ from the virtual origin to the typical distance $(M/\beta_j^{2/3})$ required for the flow to transform to the (asymptotic) plume state. The value of $(x^* - x^*_{oM})$ should therefore be equal to (or preferably, sufficiently greater than) 1 to insure that the flow has reached the asymptotic-plume state. The scaling used for the vertical coordinate M^* is suggested by equation (13). It is seen from Fig. 2(a) that the flows studied are all in the asymptotic plume state and that most of the data collapse reasonably well on to the straight line

$$M^* = (M/\beta^{2/3})\left(\frac{\beta_j^{2/3}}{M_j}\right) = \sigma_M \frac{(x - x_{oM})}{M_j}\beta_j^{2/3} = \sigma_M (x^* - x^*_{oM}) \tag{18}$$

in conformity with equation (13). A least-square fit indicates a value of 0.74 for the universal constant σ_M.

The results for the kinematic mass flux are shown in Fig. 2(b), plotted in normalized coordinates suggested by equation (12). These data also indicate the linear relation as implied by this equation, namely

$$Q^* = \left(\frac{Q}{\beta^{1/3}}\right)\left(\frac{\beta_j^{2/3}}{M_j}\right) = \sigma_Q (x^* - x^*_{oM}) \tag{19}$$

with a value of 0.48 for the universal constant σ_Q. The values of σ_M and σ_Q from [9] are 0.72 and 0.57, respectively. A growth parameter C_p defined as

$$C_p \equiv \frac{Q}{M^{1/2}(x - x_{oM})^{1/2}} \tag{20}$$

along with the Richardson number R, was introduced in [15] to characterize the plane buoyant jet. Both C_p and R attain universal values in the asymptotic plume. The value of C_p for the plume was found from their experiments to be 0.54. Now, C_p can be written as

$$C_p \equiv \left[\frac{Q}{\beta^{1/3}(x - x_{oM})}\right]\left[\frac{\beta^{1/3}(x - x_{oM})^{1/2}}{M^{1/2}}\right] = \frac{\sigma_Q}{\sigma_M^{1/2}} \tag{21}$$

Using the present values of σ_Q and σ_M, one gets $C_p \approx 0.56$ which is in reasonable agreement with the KL data.

Centerline Velocity. The asymptotic theory suggests that the centerline velocity in the plume is constant (equation 14). The results for the various plumes are shown in Fig. 3(a). It is seen from the figure that the normalized variable $U_m/\beta^{1/3}$ remains nearly constant for all the flows as implied by equation (14). There is some scatter in the data but a least-square fit indicates an average value of 2.13, with a standard deviation (indicated by the vertical bar in the figure) of 0.1. Hence,

$$\sigma_u = \frac{U_m}{\beta^{1/3}} = 2.13 \tag{22}$$

This value is significantly higher than the value of 1.66 reported by KL and the value of 1.8 reported by Rouse, Yih, and Humphreys [9]. The probable reasons for this difference, especially with the former experiments and its implications will be discussed later.

Entrainment Rate. The entrainment coefficient C_E for the asymptotic plume, can now be computed from the usual definition

$$C_E = \frac{1}{U_m}\frac{dQ}{dx} \tag{23}$$

With $\sigma_Q = 0.48$ and $\sigma_u = 2.13$, equation (23) yields: $C_E = 0.225$. Ths value is in agreement with the value of about 0.22 observed by KL and confirms the earlier conclusions of [14, 17] that the entrainment rate in a plume is nearly twice that in an isothermal jet (C_E for jet = 0.110).

Decay of Centerline Excess Temperature. It is known that the excess temperature in the asymptotic nonbuoyant jet

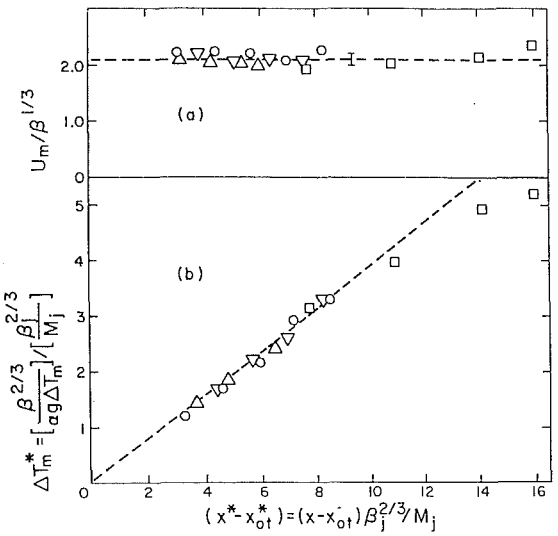

Fig. 3 Variations of centerline velocity and centerline excess temperature along the plume. Symbols as in Figs. 1. Uncertainties: x^*: ±0.3; U_m: ±0.1; ΔT_m: ±2.8 percent.

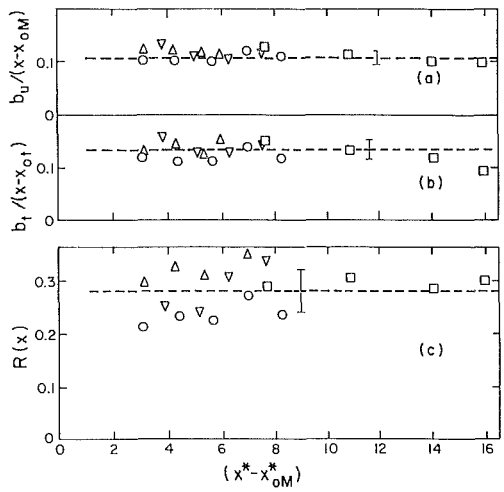

Fig. 4 Variations of the spreading rates and Richardson number Symbols as in Fig. 1. Uncertainties: x^*: ±0.3; rest shown by vertical bars.

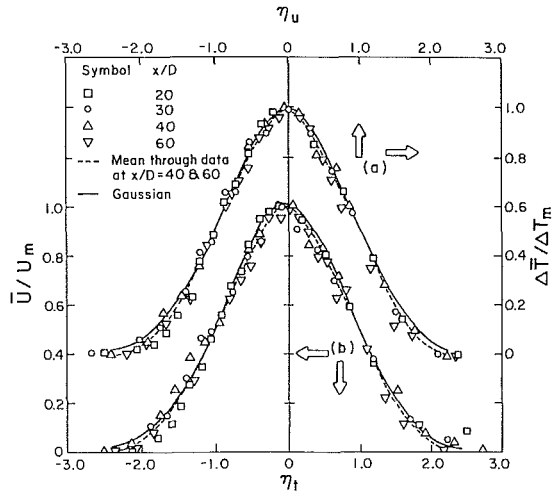

Fig. 5 Velocity and temperature distributions across the plume. Uncertainties: η: ±0.06, U: ±0.015; ΔT: ±0.015.

decays as the inverse square root of the distance from the origin [16]. The temperature-decay results for the different plumes are shown in Fig. 3(*b*), after shifting the origin (by an amount x_{ot}) as necessary in each case. This figure demonstrates that the axial temperature decays nearly as $(x^*-x_{ot}^*)^{-1}$ as indicated by equation (15). The large departure from this trend in the case of the MSC4-data is caused by contamination and possibly three dimensional effects already referred to. The temperature decay in all the flows can be approximated by the law

$$\Delta T_m^* = \left(\frac{\beta^{2/3}}{\alpha g \Delta T_m}\right)\left(\frac{\beta_j^{2/3}}{M_j}\right) = \sigma_t (x^* - x_{ot}^*) \tag{24}$$

with $\sigma_t = 0.39$. The values for σ_t reported by KL, and Rouse, Yih, and Humphreys are 0.42 and 0.385, respectively, and considering experimental uncertanties, these are not too different from the present value. It may be noted that for small temperature differences, σ_t can also be taken to be the slope corresponding to the decay of the centerline specific-weight defect, $-\Delta\gamma_m$.

Velocity and Temperature Half Widths. If the asymptotic plume is selfpreserving, it is reasonable to define, in the usual way, half widths b_u and b_t of the velocity and temperature distributions across the plume, as two characteristic length scales. They can be obtained directly from the measured velocity and temperature distributions. These data were found to exhibit very nealy linear growth rates for both b_u and b_t as indicated by equation (11). The results for the ratios, $b_u/(x-x_{oM})$ and $b_t/(x-x_{ot})$ are shown for all the plumes in Figs. 4(*a*) and 4(*b*). It may be noted that x_{oM} and x_{ot} are the same virtual origins as have already been introduced. The data show considerable scatter especially in the case of b_t, but the following average values are obtained for the growth rates

$$K_{1u} = \frac{db_u}{dx} \approx \frac{b_u}{(x-x_{oM})}$$
$$= 0.11 \text{ (with a standard deviation of 0.01)} \tag{25}$$

$$K_{1t} = \frac{db_t}{dx} \approx \frac{b_t}{(x-x_{ot})}$$
$$= 0.133 \text{ (with a standard deviation of 0.014)} \tag{26}$$

The unduly large departure, from the general trend, of the MSC4 data for K_{1t} is due to reasons already mentioned. The present values of K_{1u} and K_{1t} in reasonable agreement with the values ($K_{1u} = 0.097$ and $K_{1t} = 0.130$) reported by KL. The corresponding values of Rouse, Yih, and Humphreys [9] are $K_{1u} = 0.147$, $K_{1t} = 0.130$, but the uncertainty in their velocity measurement can be expected to be large.

Richardson Number. A significant parameter in the study of buoyant jets and plumes is the Richardson number. Figure 4(*c*) show the variation of the Richardson number $R(x)$ obtained from equation (5) using the actual values of Q, M, and b computed from the measured distribution of U, u', ΔT, and $\overline{ut}$ in the various flows. There is considerable scatter in the data, because of the uncertainties in the estimation of Q^3, M^3, and β. Nevertheless, the data for $(x^*-x_{oM}^*)$ are seen to tend toward an average value of 0.28 with a standard deviation of 0.04, as indicated by the vertical bar in the figure. Based on this and the other results presented so far, it is reasonable to state that all the flows studied have attained near-asymptotic state of turbulent plume, within the limits of experimental uncertainties.

Mean Velocity and Temperature Distributions. Profiles of the longitudinal mean velocity $\bar{U}$ and the temperature excess $\Delta\bar{T}$ are shown in Fig. 5 typically for the flow MSC3. In Fig. 5(*a*) the distributions are plotted after centering them with respect to the axis of the flow in order to correct for any small asymmetry in the flow. Also, corrections for the zero shift (in

Table 3 Turbulent properties of the asymptotic plume

Description	$\frac{u'_{cl}}{U_m}$	$\frac{v'_{cl}}{U_m}$	$\frac{t'_{cl}}{\Delta T_m}$	$\frac{\lvert\overline{uv}\rvert_{max}}{U_m^2}$	$\frac{\lvert\overline{vt}\rvert_{max}}{U_m \Delta T_m}$	$\frac{\overline{ut}_{max}}{U_m \Delta T_m}$	Pr
Plane plume present experiments)	0.275 (0.015)	0.23 (0.02)	0.42 (0.02)	0.031 (0.003)	0.045 (0.005)	0.064 (0.006)	0.46-0.70
Plane plume (Kotsovinos, [21])	0.38		0.4			0.26	
Plane nonbuoyant jet at $x/D=40$ (Ramaprian and Chandrasekhara, [16])	0.20	0.18	0.18	0.20	0.018	0.025	0.75
Predictions of plane plumes (Malin and Spalding, [6])			0.44 0.46	0.035 0.031	0.048 0.055	0.078 0.078	Variable 0.5
Axisymmetric plume (Beuther, Capp, and George, [13])	0.27	0.22	0.4	0.024	0.032	0.039-0.07	0.95

Note: cl denotes centerline values. The numbers in parentheses represent standard deviations.

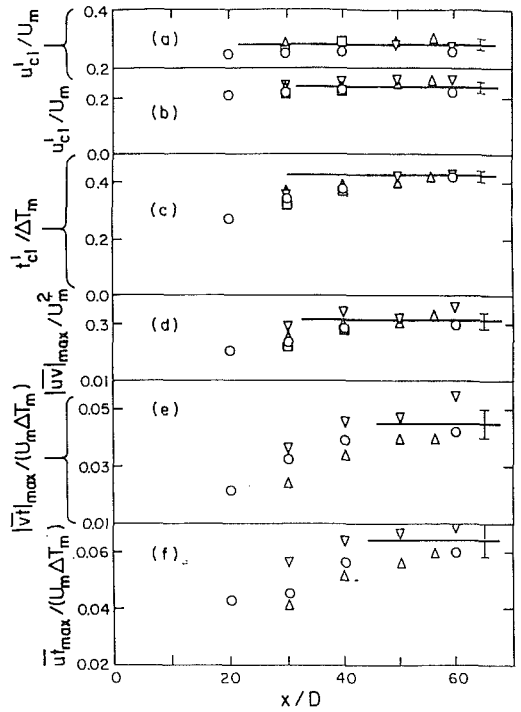

Fig. 6 Evolution of the turbulence properties along the centerline. Symbols as in Fig. 1. The horizontal line in each case is the expected asymptotic behavior. Uncertainties: shown by vertical bars.

the instrumentation) and ambient contamination have been applied (for details see [19]). The profiles show some scatter but this is acceptable considering the difficulty in making these measurements. All the profiles exhibit near-selfsimilarity for $x/D>20$. Also shown in these figures are the universal Gaussian curves

$$\frac{\bar{U}}{U_m}=\exp(-0.69\eta_u^2);\quad \frac{\Delta\bar{T}}{\Delta T_m}=\exp(-0.69\eta_t^2) \tag{27}$$

While the velocity and temperature distributions are not drastically different from Gaussian, it is possible to detect a small but consistent difference, especially in the case of the temperature distribution. Of course, there is no reason to expect that the velocity or the temperature distribution should be exactly Gaussian.

The lateral mean velocities ($\bar{V}$) were also obtained from the LDA output. These velocities were, however, very small, being of the order of 0.5-1 cm/s. The uncertainty in their determination was therefore rather large and hence are not presented here.

Turbulence Properties

Centerline and Maximum Values. The data presented so far have shown that all the flows studied have reached an asymptotic plume state in respect of the mean flow properties at $x/D\geq 30$. The axial evolution of the turbulence properties of the flow can be seen from Fig. 6. The evolution of these properties is shown in terms of the physical distance x/D instead of the normalized coordinate x^* used earlier. This is because the interest here is primarily in the (constant) asymptotic values of these properties. Furthermore, the evolution depends on the details of the turbulence structure in the boundary layers at the nozzle exit and not just on the momentum or buoyancy flux at the exit. It is seen that the centerline turbulence intensities (u'_{cl}/U_m) and (v'_{cl}/U_{max}) and the maximum Reynolds shear stress $\lvert\overline{uv}\rvert_{max}/U_m^2$ reach their respective asymptotic values (within experimental scatter) by $x/D=40$ in all the flows studied. The thermal properties such as $t'_{cl}/\Delta T_m$, $\lvert\overline{vt}\rvert_{max}/(U_m\Delta T_m)$ and $\overline{ut}_{max}/(U_m\Delta T_m)$ take longer to develop. In fact, the last two properties seem to have barely reached their terminal values at $x/D=60$. The experimental scatter is also larger in this case. It is possible that these properties are still evolving at this station. However, judging from the data trend, it seems reasonble to assume that most of the evolution has already taken place and that they tend towards the asymptotic values indicated by the horizontal lines in each figure within the uncertainty indicated by the vertical bars. Table 3 summarizes these average symptotic values along with the standard deviations. In the case of u', v', $\overline{uv}$ and t', these averages are based on the results for $40\leq x/D\leq 60$. In the case of vt and ut, these are based on the results for $50\leq x/D\leq 60$. The data from the last two stations of MSC4 have been excluded for reasons already mentioned. Table 3 also includes the available data from KL for plane plumes, data for round plumes from Beuther, Capp, and George [13] and, for comparison, the values for a nonbuoyant jet (at $x/D=40$) from Ramaprian and Chandrasekhara [16]. Lastly, the results of recent numerical calculations by Malin and Spalding [8] using a complex turbulence model (the so-called $k-\omega$ model) are also presented in the table. It can be seen that buoyancy substantially increases the turbulent intensities and turbulent transport. For example, there is a 50 percent increase in the Reynolds shear stress and about 150 percent increase in the turbulent heat fluxes in the plume relative to

the nonbuoyant jet. The table also shows that the centerline turbulent intensities u'_{cl}, v'_{cl} and t'_{cl} are approximately the same in plane and axisymmetric plumes. The maximum fluxes $|\overline{uv}|_{max}$, $|\overline{vt}|_{max}$ and $|\overline{ut}|_{max}$ are, however, about 30–35 percent higher in the plane plume. One of the two sets of results from Malin and Spalding shown in the table corresponds to a constant Prandtl number of 0.5. The other set corresponds to a variable Prandtl number. In this case, the Prandtl number was assumed to depend on a local buoyancy parameter via an empirical algebraic function. It is seen that both the numerical solutions predict the correct trends though they appear to over-predict the fluxes by 15–25 percent. The data of [14] agree with the present measurements in respect of t'_{cl} but differ significantly with regard to u'_{cl} and ut_{max}. In particular, their value of 0.26 for ut_{max} is several times larger than the typical values measured in other plume experiments (plane or axisymmetric) or predicted by numerical calculations.

Distributions of the Turbulent Properties Across the Plume. For the sake of brevity, only the distributions of the transport terms $\overline{uv}$, $\overline{ut}$ and $\overline{vt}$ across the plume are shown. Also, results are shown only for the plume MSC3, as a typical example. Similar results were obtained in other cases. The full lines are the mean (drawn by eye judgement) through the last two measurement stations. Also presented for comparison are similar results for an isothermal and a heated but nonbuoyant jet from [16]. More detailed results can be found in [18].

Reynolds shear stress: The Reynolds shear stress distributions are shown in Fig. 7(*a*). The data show acceptable symmetry and no significant scatter. Also the results for the isothermal jet agree well with those for the heated jet, thereby confirming that there are no significant effects of the refractive index fluctuations on the measurements. The measurement technique used can therefore be considered satisfactory. The peak value $|\overline{uv}|_{max}/U_m^2$ of the shear stress for the isothermal jet, as measured by the LDA is seen to be about 0.020. This is lower (by about 15–20 percent) than the value generally obtained by other investigators using hot-wire anemometry. It is, however, reasonable to compare the results obtained for the isothermal and buoyant flows from the same procedure. It is seen from Fig. 7(*a*) that the data show selfsimilarity especially beyond $x/D=40$. The shear stress values are generally much higher than those measured in the isothermal/nonbuoyant jet. As already mentioned, the measured dimensionless asymptotic peak shear stress of about 0.03 in the buoyant jet is about 50 percent higher than the corresponding value measured in the isothermal/nonbuoyant jet. The accuracy of the shear stress measurements can be assessed by examining consistency with the momentum equation. Assuming selfsimilar distributions and asymptotic growth and decay laws for b_u, U_m, and ΔT_m, the momentum equation can be integrated to obtain the distribution of $\overline{uv}$ across the plume (for details see [19]). This calculated distribution is shown by the dashed line in Fig. 7(*a*). It is seen that the shear stress distribution obtained from direct measurements is in agreement with the distribution obtained indirectly from the momentum equation within the limits of experimental uncertainty of about 10 percent. This agreement can be taken as a measure of consistency between the turbulence measurements and the mean flow measurements.

Transverse turbulent heat flux: Figure 7(*b*) shows the distributions of $\overline{vt}$, which is proportional to the transverse turbulent heat flux $\rho c_p \overline{vt}$, for the plume MSC3. While these distributions evolve more slowly than the shear stress distributions, the data for the last 2 stations exhibit a strong trend toward self-similarity. The data for the other plumes gave similar results. The figure also shows the distribution of $\overline{vt}$ in the nonbuoyant jet at $x/D=40$. It is very clear that the turbulent heat flux $\overline{vt}$ is spectacularly affected by buoyancy. Again, as in the case of the shear stress, it is possible to assess the accuracy of the turbulence heat flux measurements in the plume by comparing the measured $\overline{vt}$ distribution obtained from direct measurements with that obtained indirectly from the thermal energy equation for the plume. Integration of this equation under similar assumptions as before and using measured velocity and temperature values yields the dashed line in Fig. 7(*b*). On comparison, it is seen that the level of agreement between the direct measurement and that calculated from the thermal energy equation is poorer than in the case of shear stress. For example, the measured peak value $|\overline{vt}|_{max}/(U_m\Delta T_m)$ is on the average about 20 percent lower than the calculated value of 0.051. Part of this discrepancy is perhaps due to the fact that the flow MSC3 is possibly still evolving as is suggested by Fig. 6. It can also be seen from Fig. 6 that the flow MSC3X does indeed exhibit peak values of $|\overline{vt}|$, more nearly in agreement with the calculated value. The recommended asymptotic value of 0.045 is, however, still lower than the calculated value by about 10 percent. Some of the discrepancy may also arise from the physical separation between the points of velocity and temperature measurements.

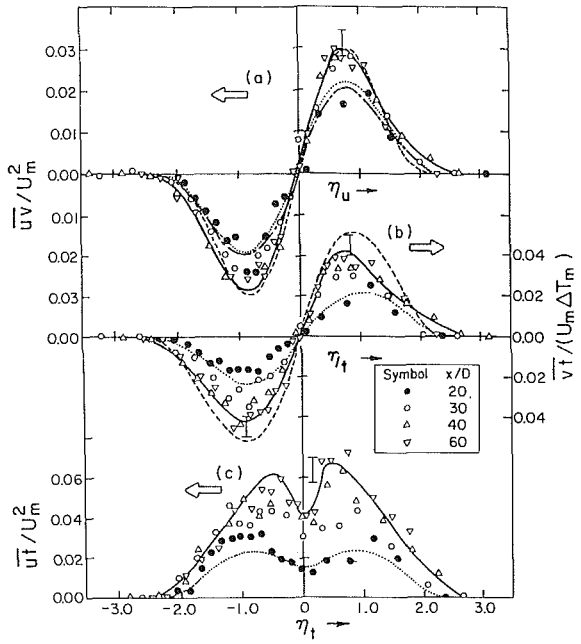

Fig. 7 Distributions of the turbuelnt transport terms across the plume MSC3. The full lines are the mean through the downstream data. The chain link and dotted lines are respectively for an isothermal and a heated but nonbuoyant jet, from [16]. The dashed lines are obtained from the momentum equation in (*a*) and the energy equation in (*b*). Uncertainties: shown by vertical bars.

Longitudinal heat flux: The distributions of $\overline{ut}$ (proportional to the longitudinal heat flux and for constant α, also proportional to the longitudinal turbulent buoyant flux) for the plume MSC3 are shown in Fig. 7(*c*). The profiles are again seen to evolve toward a self-similar state. The results for the heated nonbuoyant jet at $x/D=40$ are also shown in this figure for comparison. Again, $\overline{ut}/(U_m\Delta T_m)$ shows a drastic increase in the plume in comparison with the results for the nonbuoyant jet. The area under the $\overline{ut}$- curve for MSC3 in Fig. 7(*c*) is defined as the kinematic turbulent heat flux integral (proportional to the turbulent buoyancy flux intregral). Its magnitude is about 0.18, indicating that the total turbulent heat flux across the horizontal plane is a significant fraction of the total mean heat flux. Similar results were obtained with the other plumes also. The corresponding value for the nonbuoyant jet at $x/D=40$ is about 0.03 to 0.04. Measurements in a round plume [11, 13] also gave results similar to the present

measurements. While the effect of buoyancy on $\int \bar{u}t dy$ is thus very significant, it is not, however, as large as was measured by KL (abut 0.5 as against the present value of 0.18 for the integral).

Autocorrelation measurements of u (or v) and t signals showed that the integral length scale was several times larger than the separation between the points of velocity and temperature measurement. It was estimated from these measurements that the maximum reduction in the measured values of $\bar{vt}$ (and $\bar{ut}$), due to this separation is about 10 percent. Hence, the difference between the present heat-flux results and those of KL is likely to be due primarily to the disagreement between the velocity measurements in the two cases. The temperature measurements as well as the two-dimensionality of the flows appear to be satisfactory in both the investigations.

Detailed Structure of Turbulence

Turbulent kinetic energy balance: The turbulent kinetic energy equation for the plane buoyant jet at any axial location x can be written in the following nondimensional form using the half-width of the velocity profile and the centerline velocity as the normalizing length and velocity scales respectively [19].

$$\left[\frac{b_u}{U_m^3}\bar{U}\frac{\partial \overline{q^2}/2}{\partial x}+\frac{b_u}{U_m^3}\bar{V}\frac{\partial \overline{q^2}/2}{\partial y}\right]+\left[\frac{\overline{uv}}{U_m^2}\frac{\partial(U/U_m)}{\partial(y/b_u)}\right]-\left[\frac{\alpha g \bar{u} t b_u}{U_m^3}\right]+\left[\frac{1}{U_m^3}\frac{\partial(\overline{vq^2})}{\partial(y/b_u)}-\overline{vq^2}/2\right]+\left[\frac{1}{U_m^3}\frac{\partial(\overline{pv/\rho})}{\partial(y/b_u)}\right]+\left[\frac{\epsilon b_u}{U_m^3}\right]=0 \tag{28}$$

This equation is the same as the usual kinetic energy equation for an isothermal jet except for the additional production term due to buoyancy (fourth term). Since $\overline{w^2}$ was not measured in the experiments, q^2 was obtained from the usual assumption (see [20]),

$$\overline{q^2}=(\overline{u^2}+\overline{v^2}+\overline{w^2})=\frac{3}{2}(\overline{u^2}+\overline{v^2}) \tag{29}$$

Similarly, $\overline{q^2 v}$ was assumed to be given by

$$\overline{q^2 v}=(\overline{u^2 v}+\overline{v^3}+\overline{w^2 v})=\frac{3}{2}(\overline{u^2 v}+\overline{v^3}) \tag{30}$$

These approximations are acceptable for the purpose of comparing the essential features of jets and plumes. Some of the energy balance terms, in equation (28), were measured in the plume MSC3. These are presented and compared in Figs. 8(*a*) and 8(*b*), with the corresponding results for an isothermal jet from [16]. As is the usual convention, positive quantities in the figure denote a "loss" (or flux out of the control volume) and negative quantities denote a "gain" or flux into the control volume. It is seen that there is no significant effect of buoyancy on the diffusion term (fifth term). On the other hand, it is clear that the rate of turbulent energy production by shear (third term) is increased significantly by buoyancy. This is a direct consequence of the increase in the Reynolds shear stress in the plume, since the nondimensional velocity gradient $[\partial(\bar{U}/U_m)/\partial(y/b_u)]$ is very nearly the same in the isothermal jet and plume. In addition to this, there is also a direct production of turbulent energy by buoyancy. The total buoyant production across the plume can be estimated from Fig. 8(*b*) to be about 30 percent of the energy produced by shear. Previous studies by Kotsovinos [14] as well as the spectral and intermittency results obtained in the present study (but not presented in this paper) seem to show that the buoyant contribution occurs through the generation of large-scale eddies by gravitational disturbances. These are created by the destabilizing effect of the fluctuating buoyancy. The model suggested for this process in [21] appears to be reasonable. Buoyancy thus increases turbulent energy in two ways, directly by generating large-scale disturbances and indirectly by raising the turbulence level (and thereby the Reynolds shear stress) which in turn extracts more turbulent energy from the mean flow. The most striking difference between the jet and plume is with regard to the contribution to the turbulent energy balance by advection (first two terms in equation (28)). The advection is zero at the plume centerline and is very small in the vicinity of the centerline as opposed to large and negative values at and around the centerline of the isothermal jet. The zero advection at the plume centerline is a result of the constancy of U_m and hence of the turbulent energy $(\overline{q^2}/2)$ which scales with U_m^2 in the x-direction. In a jet on the other hand, the turbulent energy at the centerline decays as x^{-1}. In fact, a study of the continuity requirement would show that the streamlines in the plume are convergent everywhere except at the centerline where they are parallel. In the jet, the streamlines are convergent in the outer regions and divergent in the central part. The difference between the advection curves in the jet and plume is predominantly due to this difference in their streamline patterns.

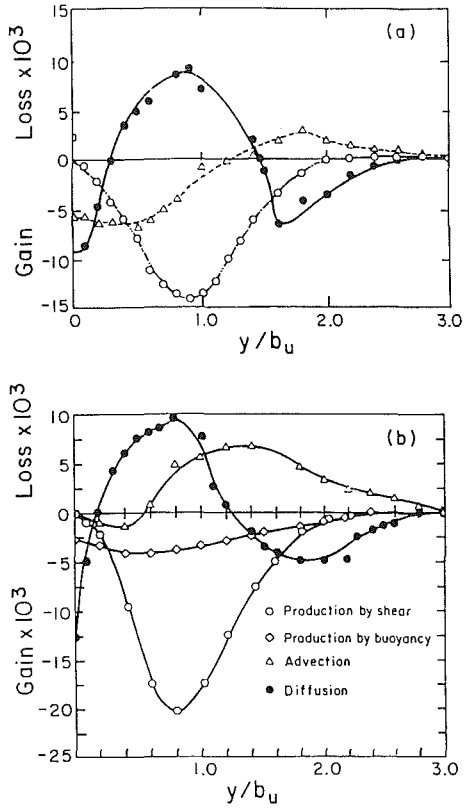

Fig. 8 Comparison of the energy balance terms form equation (26) for the plume MSC3 with the isothermal jet of [16]. (*a*) isothermal jet; (*b*) plume. Uncertainties: y/b_u: ± 0.06; Production: ± 15 percent; Advection: ± 15 percent; diffusion: ± 20 percent; [best estimates].

Conclusions

1. The study confirms many of the results from earlier studies on the asymptotic two-dimensional plume. For example, the study has confirmed that all plane buoyant jets reach a universal asymptotic state in respect of both the mean and tur-

bulent flow properties. However, the present mean-flow measurements, while indicating the constancy of U_m and Richardson number R in the asymptotic plume, yield larger values for U_m (and hence, for R) than measured by Kotsovinos and List [15]. Future experiments will hopefully resolve this difference.

2. Buoyancy causes a significant increase in the turbulent intensities and turbulent fluxes and transport coefficients. The order of increase observed in the present experiments is similar to that observed by Beuther, Capp, and George in round plumes [13], but significantly smaller than that observed in [15].

3. The turbulent kinetic energy balance shows increased production by Reynolds shear stress and also significant buoyant production near the central region of the plume. Production from these two sources is responsible for the sustenance and enhancement of turbulence in the plume.

Acknowledgment

The study reported in this paper was supported by the U.S. National Science Foundation under Grant Nos. ENG77-22756 and CME 80-06797. This support is gratefully acknowledged.

References

1 Priestly, C. H. B., and Ball, F. K., "Continuous Convection from Isolated Source of Heat," *Quart. J. Roy. Met. Soc.*, Vol. 81, 1955, pp. 144–157.

2 Morton, B., Taylor, G. I., and Turner, J. S., "Turbulent Gravitational Convection From Maintained and Instantaneous Sources," *Proc. Roy. Soc.*, Vol. A234, 1956, pp. 1–23.

3 Fan, L. N., and Brooks, N. H., "Numerical Solutions of Turbulent Buoyant Jet Problems," W. M. Keck Laboratory of Hydraulics and Water Resources Report No. KH-R-18, California Institute of Technology, Pasadena, 1969.

4 Brooks, N. H., and Koh, R. C. Y., "Discharge of Sewage Effluent From a Line Source Into a Stratified Ocean," Eleventh Congress of Int. Assoc. for Hydraulic Research, Paper No. 2.19, 1965.

5 Madni, I. K., and Pletcher, R. H., "Prediction of Turbulent Forced Plumes Issuing Vertically Into Stratified or Uniform Ambients," ASME *Journal of Heat Transfer*, Vol. 99, No. 1, 1976, pp. 99–104.

6 Chen, C. J., and Rodi, W., "A Mathematical Model For Stratified Turbulent Flows and Its Application to Buoyant Jets," Paper C4, 16th Congress of the Int. Assoc. of Hyd. Research, Sao Paulo, Brazil, 1975.

7 Hossain, M. S., and Rodi, W., "A Mathematical Model for Buoyant Flows and Its Application to Vertical Buoyant Jets," *Turbulent Jets and Plumes*. ed. W. Rodi, Pergamon Press, Oxford, 1982.

8 Malin, M. R., and Spalding, D. B., "The Prediction of Turbulent Jets and Plumes by Use of the k-ω Model of Turbulence," *Physiochemical Hydrodynamics*, Vol. 5, No. 2, 1984, pp. 153–198.

9 Rouse, H., and Yih, C. S., and Humphreys, H. W., "Gravitational Convection From a Boundary Source," *Tellus*, Vol. 3, 1952, pp. 201–210.

10 Lee, S. L., and Emmons, H. W., "A Study of Natural Convection Above a Line Fire," *J. Fluid Mech.*, Vol. 11, 1961, pp. 353–368.

11 Nakagome, H., and Hirata, M., "The Structure of Ambient Diffusion in an Axisymmetric Thermal Plume," *Proc. Int. Conf. on Heat and Mass Transfer*, Seminar on Turbulent Buoyant Convection, Dubrovnik, Yugoslavia, 1976, pp. 361–372.

12 George, W. K., Alpert, R. L., and Tamanini, F., "Turbulence Measurements in an Axisymmetric Buoyant Plume," *Int. J. Heat and Mass Transfer*, Vol. 20, 1977, pp. 1145–1154.

13 Beuther, P. D., Capp, S. P., and George, W. K., Jr., "Momentum and Temperature Balance Measurements in an Axisymmetric Turbulent Plume," ASME Paper No. 79-HT-42, Joint ASME/AIChE 18th National Heat Transfer Conference, San Diego, California, Aug. 6–8, 1979.

14 Kotsovinos, N. E., "A Study of the Entrainment and Turbulence in a Plane Buoyant Jet," W. M. Keck Laboratory of Hydraulics and Water Resources Report No. KH-R-32, California Institute of Technology, Pasadena, 1975.

15 Kotsovinos, N. E., and List, E. J., "Plane Turbulent Buoyant Jets. Part I. Integral Properties," *J. Fluid Mech.*, Vol. 81, Part 1, 1977, pp. 25–44.

16 Ramaprian, B. R., and Chandrasekhara, M. S., "LDA Measurements in Plane Turbulent Jets," ASME JOURNAL OF FLUIDS ENGINEERING, Vol. 107, 1985, pp. 264–271.

17 List, E. J., "Turbulent Jets and Plumes," *Ann. Rev. Fluid Mech.*, Vol. 14, 1982, pp. 189–212.

18 Ramaprian, B. R., and Chandrasekhara, M. S., "Study of Plane Turbulent Jets and Plumes," IIHR Report No. 257, The Institute of Hydraulic Research, University of Iowa, Iowa City, Iowa, 1983.

19 Chandrasekhara, M. S., "Study of Vertical Plane Turbulent Jets and Plumes," PhD thesis, Mechanical Engineering Department, University of Iowa, Iowa City, Iowa, 1983.

20 Bradshaw, P., "The Turbulence Structure of Equilibrium Boundary Layers," *J. Fluiid Mech.*, Vol. 29, 1967, pp. 625–645.

21 Kotsovinos, N. E., "Plane Turbulent Buoyant Jets. Part 2. Turbulence Structure," *J. Fluid Mech.*, Vol. 81, Part 1, 1977, pp. 45–62.